Ohmic Contact to Two-Dimensional Nanofabricated Silicon Structures with a Two-Probe Scanning Tunneling Microscope

Jo Onoda,[*,†] Ali Khademi,[‡] Robert A. Wolkow,[†,¶] and Jason Pitters[§]

†*Department of Physics, University of Alberta, Edmonton, Alberta T6G 2J1, Canada*

‡*Metrology Research Centre, National Research Council of Canada, 1200 Montreal Road, Ottawa, ON K1A 0R6, Canada*

¶*Quantum Silicon, Inc., Edmonton Alberta T6G 2M9, Canada*

§*Nanotechnology Research Centre, National Research Council Canada, Edmonton, Alberta T6G 2M9, Canada*

E-mail: jonoda@ualberta.ca

Role of Insulating Trench Areas

Here, we discuss the role of insulating trench areas, especially if they have significant effects on the conduction at the surface and space-charge layers. Figure S1(a) shows schematics of conduction at Si(111)-(7×7) surface layer, space-charge layer, and bulk, respectively, in the configuration of our Ohmic 1P-STM. The thickness of the topmost surface layer is monoatomic (∼1 nm) and the surface states conduction is supposed to occur at this layer. As discussed in the main text, when some electrons are transferred from the bulk into the surface states because of the charge neutrality rule between surface and bulk, the space-charge layer is formed as carrier depletion region, forming upward band bending. The sophisticated three-layer model for conductance finds that the thickness of the space-charge layer is 0.9 μm with the conductivity of 1.5×10^{-4} S/m for a n-doped Si(111)-(7×7) sample with nominal bulk resistivity of 20 Ωcm.[1] Since our n-doped Si(111)-(7×7) samples have nominal bulk resistivity of 5 Ωcm, thickness and conductivity of the space-charge layer could become slightly smaller values but still in the same magnitude. The thickness of the bulk is typically more than 100 μm for samples cut from commercial Si wafers. Figure S1(b) shows the schematics with insulating trench area, which surrounds a specific surface domain. As discussed in the main text, it is experimentally clear that the trench lines electronically decouple the inside surface layer from otherwise Si surface, thus suppressing surface states conduction (Fig. S1(b)). One of concerns in making trench lines is the contamination of the Si surface inside the trench areas. As shown in Fig. S1(c), when we have relatively sharp tip apex, it is possible for the inside surface area to be almost intact, although the ejected Si atoms tend to be adsorbed around the trench lines. Typically, surrounding some areas with more than 50 nm in width and length is enough to ensure cleanliness of the isolated surface area. Another concern is related to the effect of the trench lines on the space-charge layer. Considering how the space-charge layer originates and how wide its thickness is (typically 1 μm), it is less likely that the trench lines fabricated at the surface layer have significant effect on the potential at the space-charge layer. Thus, it can be assumed that conduction

at the space-charge layer does not change much after the trench fabrication (Fig. S1(b)). These are the important factors that decide if we can do the subtraction method to deduce surface conductance as discussed in Further Discussion of Ohmic 2P-STM in Supplementary Information.

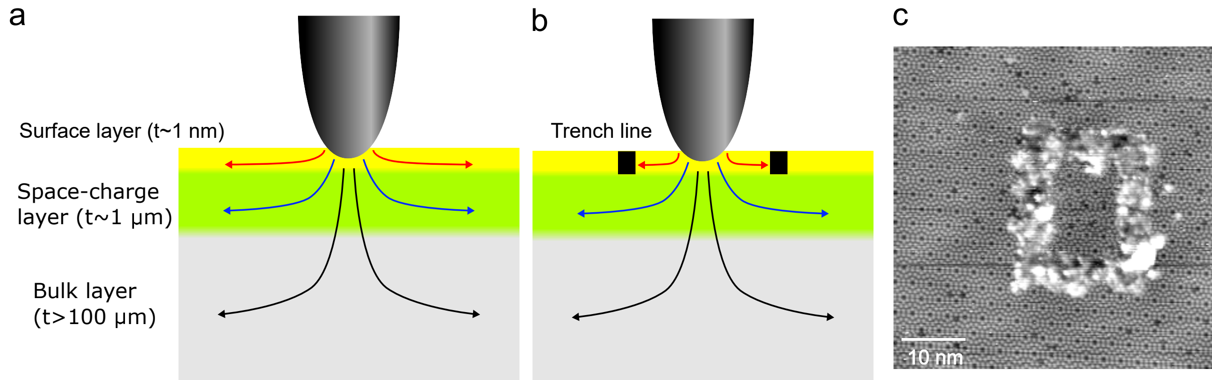

Figure S1: Schematics of the conduction at Si(111)-(7×7) surface layer, space-charge layer, and bulk layer. Parallel conduction channels when the probe is located outside (a) and inside (b) of the area restricted by the trench lines. (c) STM image of the box-shaped area obtained with $V_{1P} = +2$ V and $I_t = 20$ pA.

Nano-Schottky Contact

It is known that electrical transport through metal-semiconductor interfaces show rectifying characteristics in I-V curve. The potential barrier formed at a metal-semiconductor junction is called a Schottky barrier. For simplicity, first we assume the contact between planar metal electrode and the semiconductor surface without surface states (*e.g.* hydrogen-terminated Si(100) surface), where the work function of the metal is higher than that of the semiconductor. When they touch each other without any applied bias voltage, electrons are transferred from the semiconductor to the metal and then form upward band bending (depletion layer) toward the metal (Fig. S2(a)). The width of the depletion layer (W_{d}) can be characterized as $W_{\mathrm{d}} = \sqrt{\frac{2\varepsilon_r \varepsilon_0 (\Phi_{\mathrm{S}} - E_{\mathrm{C}} + E_{\mathrm{F}})}{e^2 N_{\mathrm{d}}}}$, where ε_{r} (ε_0) is relative (vacuum) permittivity, Φ_{S} is Schottky barrier height, E_{C} is conduction band minimum, E_{F} is Fermi level, e is elementary charge, and N_{d} is the dopant density. This type of the first approximation is so-called a Schottky-Mott model (or Schottky limit) and predicts the existence of band bending in a semiconductor, where Φ_{S} varies with strongly with the characteristics of the metal. The transport property of such a "macro-Schottky contact" without surface states is described by the thermionic emission (I_{therm}) and given by the following equation:

$$I_{\mathrm{therm}} = A A_R^* T^2 \exp\left(-\frac{e\Phi_{\mathrm{S}}}{k_B T}\right)\left(\exp\left(\frac{eV}{\eta k_B T}\right) - 1\right), \tag{1}$$

where A is the area of the metal-semiconductor contact, A_R^* is the effective Richardson constant, T is the temperature, k_B is the Boltzmann constant, V is the bias voltage, and η is the ideality factor.[2]

Figure S2(c) shows a schematic of I-V characteristic for the macro-Schottky contact, where the current in the reverse bias is almost negligible and that in the forward bias is dominant. This is categorized as conventional rectification behavior. On the other hand, when the size of the metal–semiconductor interface is smaller than W_{d}, the transport property is affected largely by the size and shape of the metal electrode. In this regime of a "nano-

Schottky contact" without surface states, I-V characteristic deviates from the conventional thermionic emission. The resulting thin barrier in small diodes will give rise to enhanced tunneling emission (I_{tunnel}), which is given by

$$I_{\text{tunnel}} = A\frac{e^2 E_{\text{max}}^2}{8\pi h \Phi_{\text{S}}} \exp\left(-\frac{8\pi}{3heE_{\text{max}}}\sqrt{2m^*\left(e\Phi_{\text{S}}\right)^3}\right), \tag{2}$$

where E_{max} is the maximum electric field at the interface, h is the Planck constant, and m^* is the effective electron mass. Thus, the electrical conduction of nano-Schottky contact is described by the sum of those emissions: $I_{\text{therm}} + I_{\text{tunnel}}$. Figure S2(c) represents a schematic of I-V characteristic for the nano-Schottky contact, where the current in the reverse bias is dramatically enhanced due to the tunneling emission (reverse rectification). In Ref. 3, the evolution of nano-Schottky behavior from the reverse rectification behavior, where the contact radius (r) is 7 nm, to the conventional rectification behavior, where $r = 100$ nm, is demonstrated by the simulation. However, when we have a Si sample with higher dopant concentration, W_{d} becomes smaller and the electric field generated by the nano-size electrode can be screened more by carriers. Thus, the I-V characteristic with highly doped sample would result in conventional rectification behavior in spite of nano-Schottky contact.[4] When there are interface states at the metal-semiconductor interfaces and/or surface states of semiconductor, the situation becomes more complicated. It is found experimentally that the Schottky-Mott model would give incorrect predictions for the height of Φ_{S} in macro-Schottky contacts.[2] This phenomenon is referred to as "Fermi level pinning", rendering Φ_{S} insensitive to the metal's work function (this is so-called Bardeen limit).

Our Ohmic 1P-STM on the Si(111)-(7×7) surface outside of the confined area made by trench lines (thus bare Si surface areas) corresponds to the case of the nano-Schottky contact with surface states. While the electric field stemming from the tip surface away from the contact region could be screened by the metallic surface states, the electric field right beneath the contact region would not be screened efficiently, thus presumably being described as the

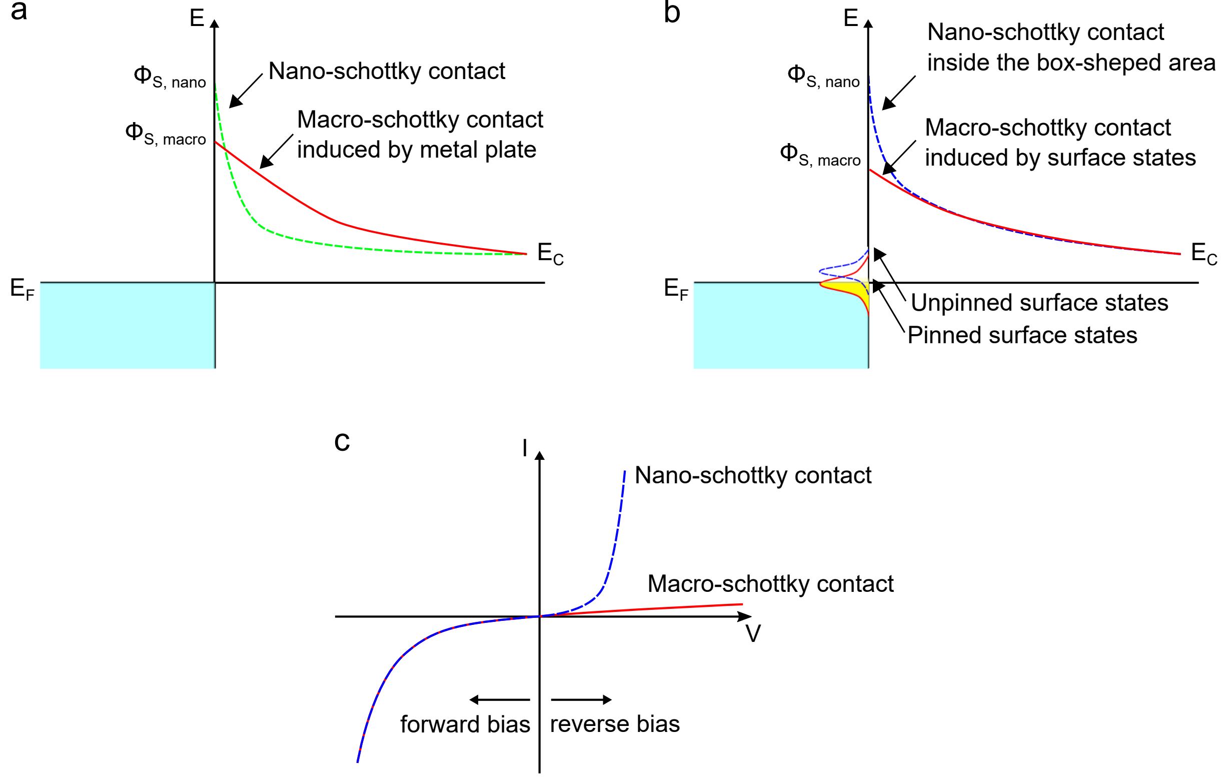

Figure S2: Comparison of the macro- and nano-Schottky contacts. (a) Potential profiles of macro- and nano-Schottky contacts without surface states. (b) Potential profiles of macro-Schottky contact with pinned surface states and nano-Schottky contact with unpinned surface states. (c) I-V characteristic of macro- and nano-Schottky contacts.

case of the nano-Schottky contact in Fig. S1(a). As discussed in Role of Insulating Trench Areas in Supplementary Information, there is a space-charge layer beneath the surface with about 1 μm thickness. While the nano-Schottky contact would give rise to local modification of potential barrier, the space-charge layer induced by the Si(111)-(7×7) surface would cause global offset in Φ_S as shown in Fig. S2(b). Because of the large contribution of the surface states conduction to the total conduction, it is hard to observe the I-V characteristic of the nano-Schottky contact when the probe is contacted outside the confined areas. It, however, becomes possible to measure it inside the confined areas as realized in the I-V curves obtained on the isolated Si(111)-(7×7) box (Fig. 2(a)) and wires (State 3 and 4 in Fig. 5). The I-V curves inside the confined areas show the reverse rectification behavior of the nano-Schottky contact, where the current in the reverse bias is dramatically enhanced due to the tunneling

emission. Since we used low doped Si samples (10^{15} atom $\cdot$ cm^{-3}) in our experiments, W_{d} could become large and thus the condition for nano-Schottky contact would be met.

The I-V characteristic of the nano-Schottky contact (normal or reverse rectification behavior) could affect a STM image contrast at the confined area. In Ref. 5, the dark depression was observed at the confined area when the positive sample bias was applied. In contrast, in our case, the confined area appears darker at negative sample bias (Figs. S3(a) and (b), the same box-shaped area in Fig. 2(a)). The I-V curves obtained at tunneling regime (parameters:) for the inside and outside of the box-shaped area are shown in Fig. S3(c), which show the similar trend of the I-V curves acquired at contact regime in Fig. 2(c) (reverse rectification behavior). The main difference between the previous[5] and the present studies is the dopant concentration of the Si sample; while the sample used in the former was highly doped ($\sim 1\times10^{19}$ atom$\cdot$cm^{-3}), the sample in the latter is low doped ($\sim 1\times10^{15}$ atom$\cdot$cm^{-3}). As discussed above, highly doped sample would show normal rectification behavior, thus resulting in the darker STM contrast at the confined area with positive sample bias in Ref. 5.

We also show I-V curves measured on the bare Si surface by 1P-STM with different tip insertion depths of -200 pm, -300 pm, and -1 nm in Fig. S3(d). The conductance for these insertion depth becomes 3.3×10^{-9} S, 7.9×10^{-9} S, and 1.4×10^{-6} S, respectively. We found that the variation of conductance as a function of tip-sample distance almost perfectly follows the previous trend for Si(111) (Fig. 10 in Ref. 6). This can be a proof that tips directly contact with the sample when we measured I-V curves with 1P- and 2P-STM.

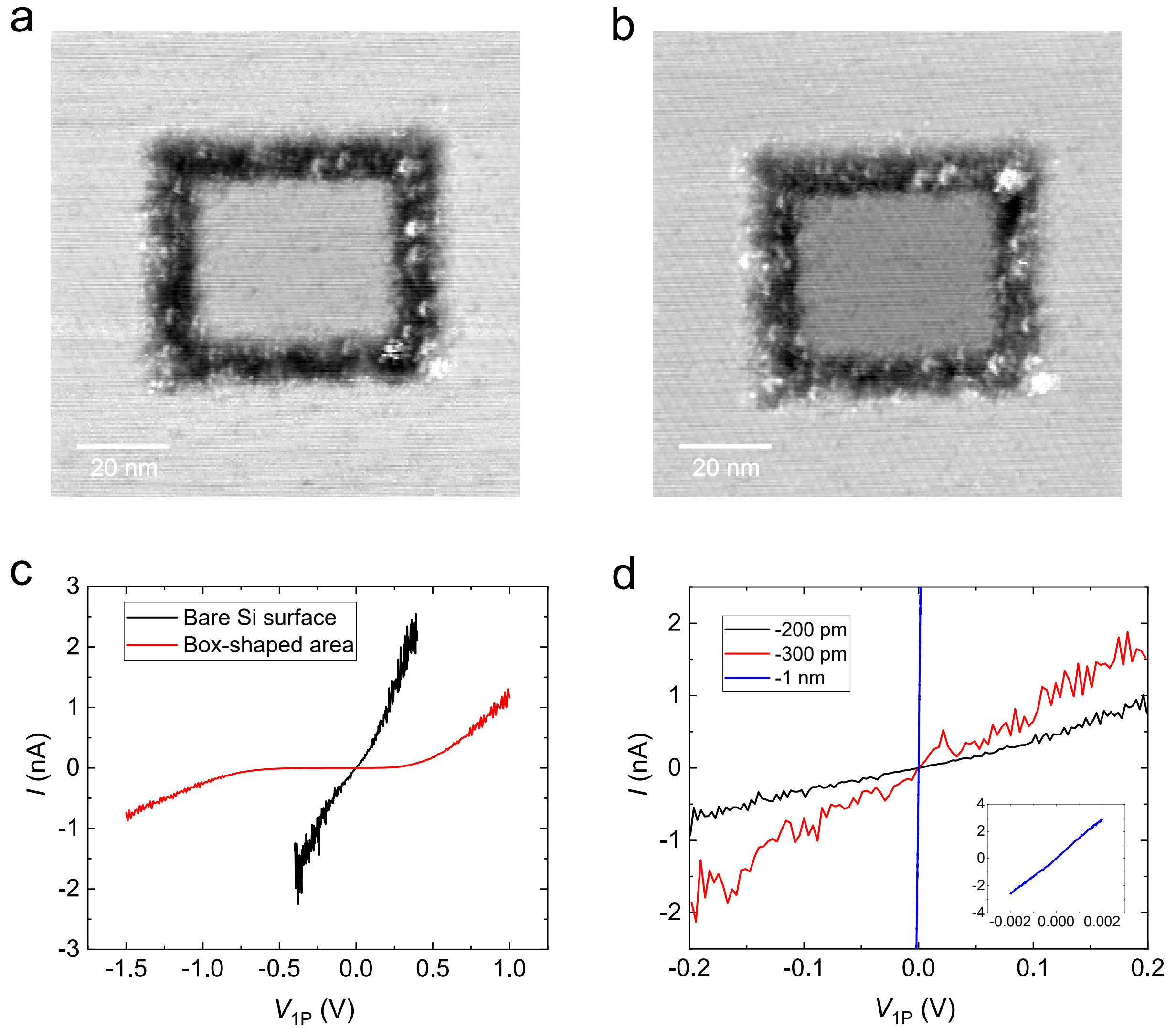

Figure S3: Effects of the reverse rectification behavior on the STM contrast. STM images of the box-shaped area obtained with I_t = 1 nA and V_{1P} = +2 V (a) and -2 V (b). (c) 1P I-V curves obtained at bare Si surface and inside of the box-shaped area with the insertion depth of -200 pm. (d) Comparison of 1P I-V curves with different insertion depths of -200 pm, -300 pm, and -1 nm. Inset shows the magnified I-V curve for -1 nm. The tip insertion of the 1P I-V measurements for (c) and (d) were carried from the height for STM set-point (V_{1P} = -2 V and I_t = 20 pA).

Further Discussion of Ohmic 2P-STM

Resistance measurement with variable probe distance is often conducted to evaluate the contribution of the surface conductance to the total conductance.[7,8] Using this method, we are able to extract the surface conductivity of the Si(111)-(7×7) surface as shown in Fig. 2(d). Another method is to measure the conductance change before and after the surface passivation with molecules such as O_2[9] or 1,2,4-Trimethylbenzene.[10] Basic assumption is that the only surface states is quenched by dosing, and that conductance at space-charge and bulk layers do not change significantly. However, as discussed in Role of Insulating Trench Areas in Supplementary Information, the band bending at the space-charge layer is sensitive to the condition of surfaces, thus the passivation method would lead to a change in the contribution of the space-charge layer. Specifically for the Si(111)-(7×7) surface, the change in the conductivity of the space-charge layer is complicated, since the Fermi energy of the surface states, which is initially pinned, would become unpinned even before the completion of the surface passivation, and the degree of the band bending would keep changing until the surface is completely covered with the reactants.

Contrary to the surface passivation method, electronically decoupled areas, which are fabricated by insulating lines such as trench lines on the Si(111)-(7×7) surface or hydrogen-passivation lines on the Si(100) surface,[11] are less influential on the space-charge layer as discussed in Role of Insulating Trench Areas in Supplementary Information. Figures S4(a) and (b) show schematics of the conduction at surface states layer, space-charge layer, and the bulk layer with the probes of 2P-STM inside and outside the electronically decoupled areas; I-V curves 1 and 2 respectively. As long as the tip-to-tip separation distance is longer than the separation distance between the points of tip-to-sample contacts for the inside and outside of the confined area ($\sim$ 100 nm in the case for Fig. S4(d)), we are able to assume that only the surface states conduction is suppressed and other conduction of the space-charge layer and bulk layer does not change significantly. Thus, it is possible to carry out the subtraction between the I-V curves 1 and 2, resulting in the I-V curve 3 in

Fig. S4(c) which is considered to contain only the surface states contribution. Note that Fig. S4(c) shows the possible conduction transitions between the charge transport channels as well. Using this subtraction method, it might be possible to apply our conductance measurement with Ohmic 2P-STM to less conductive surface states (*e.g.* semiconducting surface states), where the surface can have lower conductivity than the space-charge layer and the bulk layer. In addition, this method will also have to be considered when we conduct the conductance measurement with a larger tip-to-tip separation distance since the conduction interchangeable between the layers is more likely to happen during the transverse conduction (Fig. S4(c)).

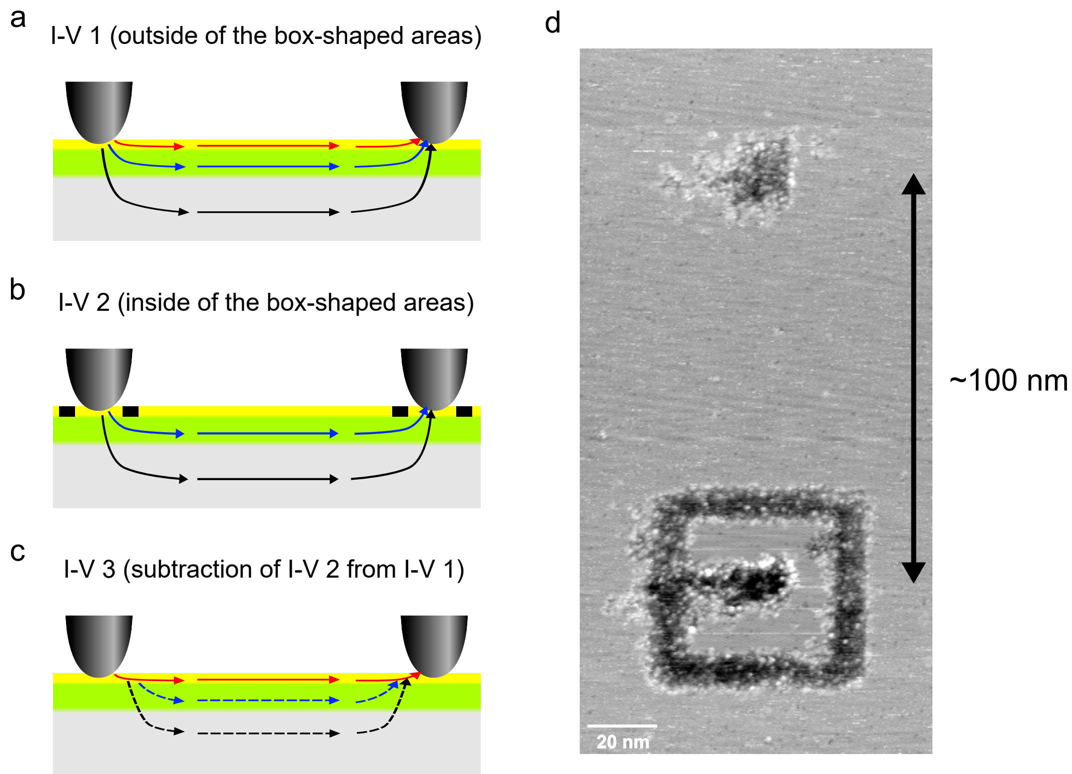

Figure S4: Extraction of surface conduction using the subtraction method. Schematics of I-V measurements carried out outside (a, I-V curve 1) and inside (b, I-V curve 2) of the electronically decoupled area. (c) I-V curve 3 obtained by subtracting I-V curve 2 from I-V curve 1. (d) STM image of the contacted areas outside and inside of the confined area fabricated by the trench line.

Trial of the Surface Conductance Evaluation with Non-Ohmic Contacts

When the apices of the two probes are covered with less-conductive materials (*e.g.* Si layers) as shown in Fig. S5(a), I-V curves obtained with 2P-STM show non-Ohmic behavior (Fig. 1(e)). Even with such non-Ohmic contacts, it might be possible to obtain the order of magnitude of the surface conductance using the following method. Figure S5(b) shows the energy diagram of non-Ohmic 2P-STM during the conductance measurement, where two tunneling barriers are inserted between the individual probes and sample. When the probes and the surface states are metallic, we can assume double Schottky barriers at each tip-to-surface contact as show in Fig. S5(b). As discussed in Nano-Schottky Contact in Supplementary Information, these can be characterized by the nano-Schottky contact with barrier height of Φ_S. For simplicity, we assume all the interfaces have the same Φ_S. In the case of $V_{2P} < 4(\Phi_S/e)$, the behavior of the I-V curve would be described by the sum of thermionic and tunneling emissions for the individual interfaces, which results in the non-linear behavior in Fig. 1(e). On the other hand, when we apply the bias voltage of $V_{2P} > 4(\Phi_S/e)$ for the quadruple nano-Schottky contacts, the I-V characteristic could be reduced to simple Ohmic behavior.[12] The differential conductance (dI/dV) for $V_{2P} > 4(\Phi_S/e)$ would give us the conductance which is comparable to that obtained by Ohmic 2P-STM. Since Φ_S is typically 0.7 eV, the bias range of $|V_{2P}| > 2.8$ V would be necessary. It should, however, be considered as well that there must be the leak current toward the space-charge layer and the bulk layer at this bias window. In order to tackle this issue, we can utilize the electronically decouple areas as discussed in Further Discussion of Ohmic 2P-STM in Supplementary Information. Figure S5(c) shows I-V curves measured with non-Ohmic 2P-STM with individual two probes inside and the outside the areas confined by trench lines (both of them are similar to the one in Fig. S4(d)). We subtracted the component for the inside of the trench boxes from the one for the outside of them and then obtained the I-V

curve which contains the surface contribution dominantly. By assuming the 2D resistance $R = \frac{1}{\pi\sigma_S} \ln \frac{L-r}{r}$, where σ_S is surface conductivity, L is tip-to-tip separation distance, and r (= 10 nm typically) is the contact radius, we obtained $\sigma_S = 5.7 \times 10^{-6}$ S/□, which is comparable with the ones obtained with our Ohmic 2P-STM and 4P-STM in the literature. However, it should be noted that this conductivity evaluation method could be useful for the conductive surfaces such as a bare Si(111)-(7×7) surface but not for less conductive ones such as the confined areas. This is because the ratio of the surface contribution to the total one becomes less and then cause a large error in the subtracted curve.

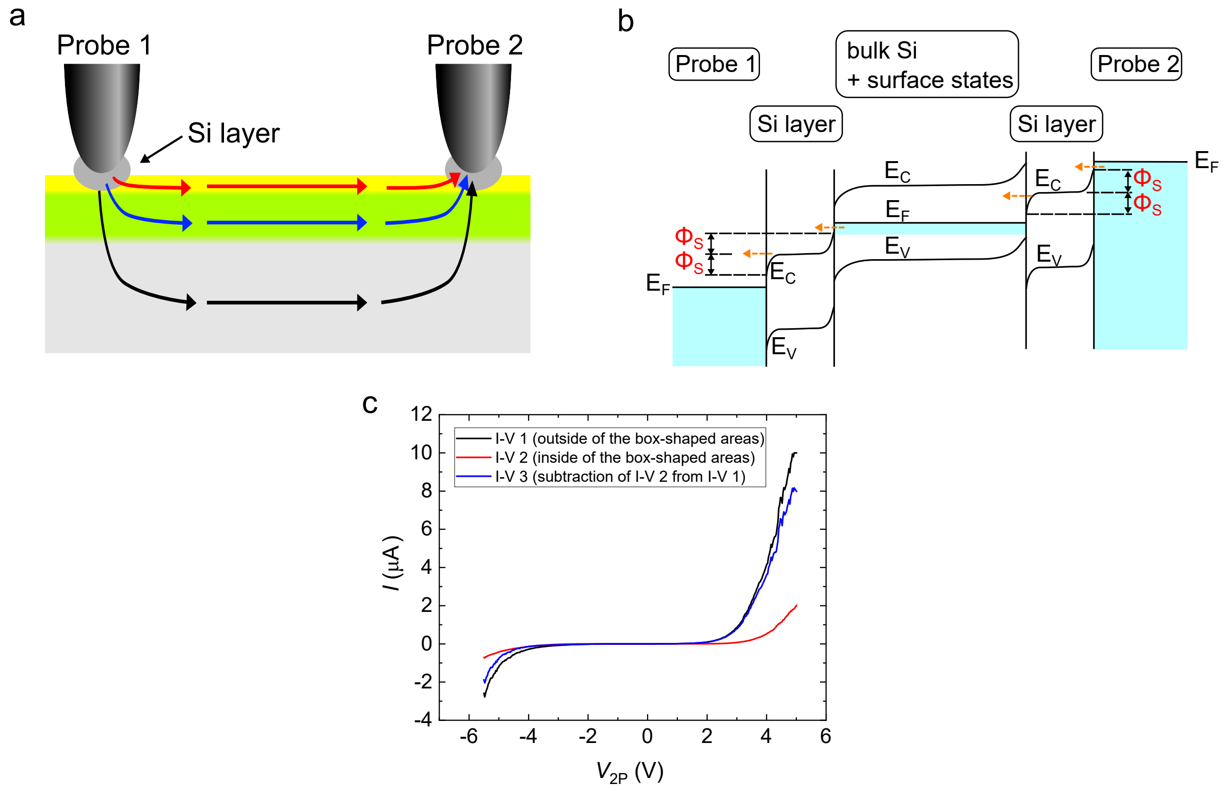

Figure S5: Measurements of surface conduction with non-Ohmic contacts. (a) Schematics of 2P I-V measurements with Si layer at the tip apex. (b) Energy diagram of the non-Ohmic 2P-STM in the case of $V_{2P} > 4(\Phi_S/e)$. (d) Subtraction method to extract surface conduction with non-Ohmic contacts.

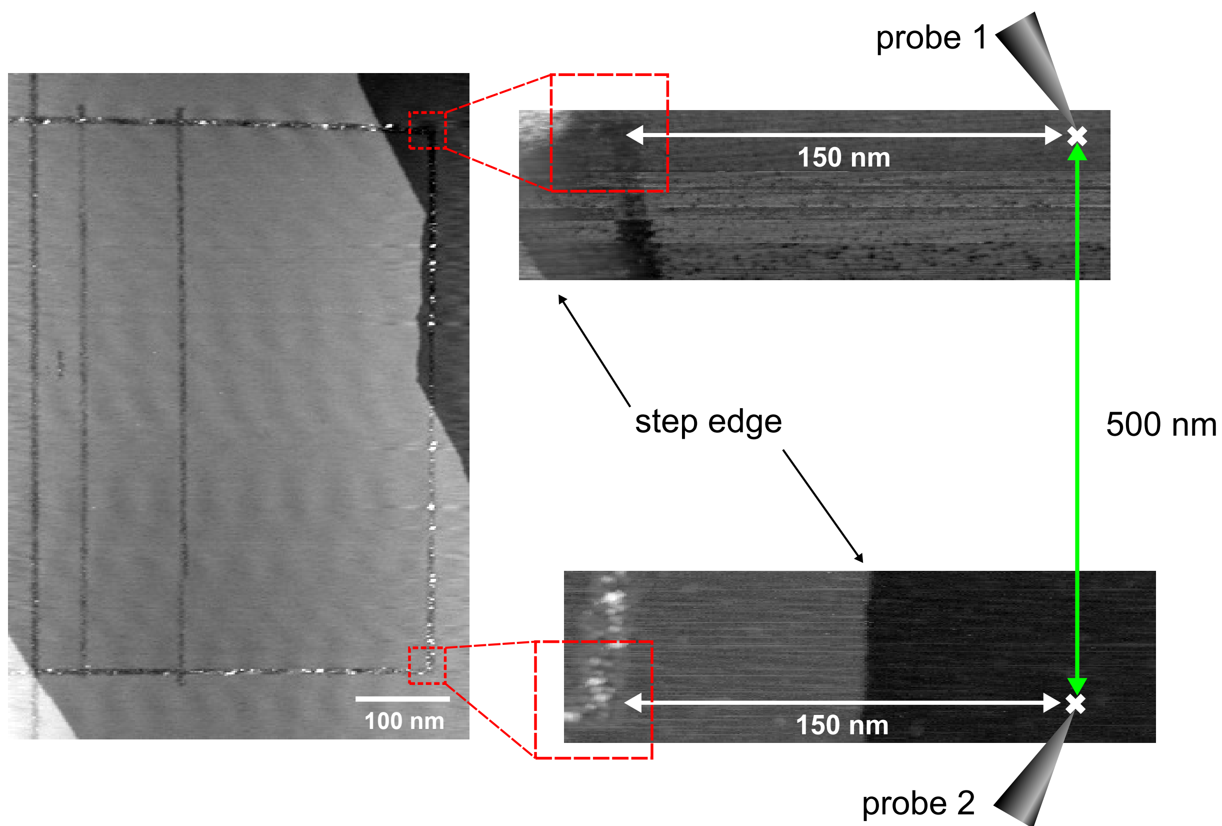

Figure S6: STM images of the measured areas for the I-V curve of Si bare surface in Fig. 3(b). The measured areas are located on the lower terrace.

Guiding of Two Probes Using the Long Trench Wire

When we conducted 2P-STM measurements with the tip-to-tip separation distance of less than 1 μm, we utilized a long trench wire for guiding of the two probes. Note that because the STM unit is suspended with springs and the mechanical vibration causes worsening of SEM resolution (about 1 μm), it is hard to finely guide the probes only with SEM. First we fabricated a 1 μm-long trench wire with V_{1P} = -3 V and It = 300 nA with probe 2 as shown in Figs. S7(a) and (b). After finishing the fabrication of the long trench wire, we kept probe 2 at the terminal of the wire (Fig. S7(c)) and place probe 1 as close to probe 2 as possible using SEM. Then, we started exploring the other terminal of the wire with probe 1 (Fig. S7(c)). In order to effectively find the terminal, we set the imaging condition of V_{2P} = 2 V and I_t = 1 nA, at which the trench wire can be imaged as a depressed region (200 – 300 pm lower from the otherwise clean Si(111)-(7×7) surface), and scanned the surface with a relatively large width (500 nm – 1 μm) (Fig. S7(c)). Once we find the other end of the wire with probe 1, we make probe 1 carefully approach to probe 2 along the long trench wire. At some point, probe 1 touches with probe 2, indicating that they are separated with the closest distance (typically 100 – 300 nm). After finishing the fine guidance of the two probes, we moved them to other clean areas while keeping their separation distance and then prepared some other trench lines necessary for conducting 2P-STM experiments. We did the same method when we conducted the experiments related to Figs. 3 in the main text. As demonstrated in Ref. 13, a 1 μm-long DB wire on the hydrogen-terminated Si surfaces can play the same role of the trench wire.

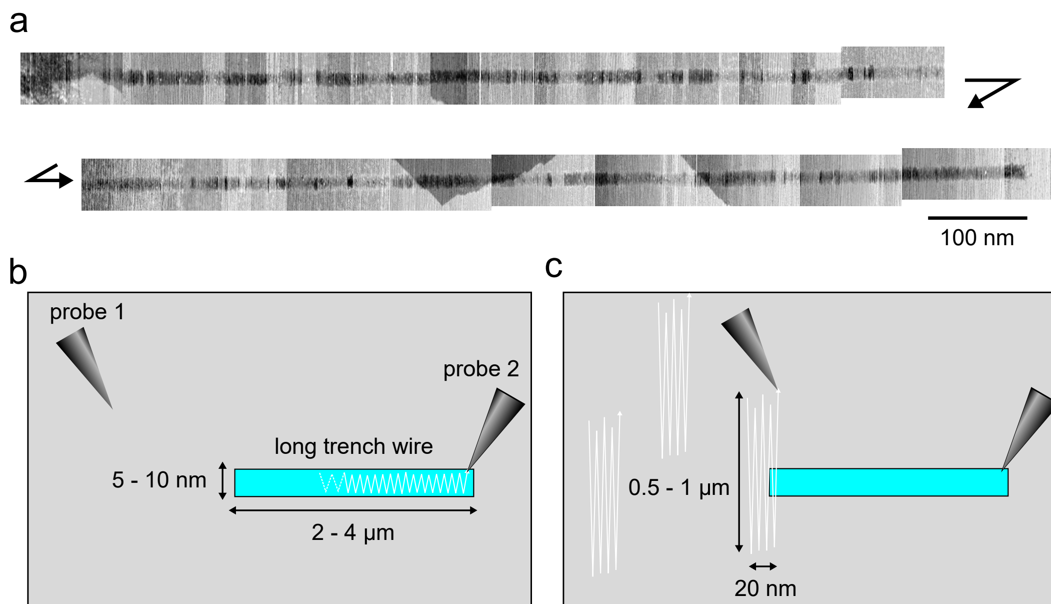

Figure S7: The method to guide two probes within 1 μm. (a) STM image of the long trench wire. Schematics of the fabrication of the long trench wire with probe 2 (b) and the exploration of the wire with probe 1 (c).

Correspondence between 2P-STM with 1P-STM upon the Conductance Measurement

Here, we discuss the equivalence between 2P- and 1P-STM on the conductance measurement of the U-shaped wire on the Si(111)-(7×7) surface (Fig. 4). It should be noted that this equivalence is achieved only when the bare Si surface is more conductive than the confined area, meaning $R_1 > R_2$ in Fig. 4(c). We prepared another U-shaped wire (950 nm in length) as shown in Fig. S9(a) and placed probe 1 500 nm apart from the open end of the wire (thus the total tip-to-tip separation distance was 1450 nm). First, we positioned probe 2 outside the U-shaped wire (Fig. S9(a)) and compared I-V curves with three different setups; 2P-STM with sample open (Fig. S8(a)), 2P-STM with sample closed (Fig. S8(c)), and 1P-STM with sample closed (Fig. S8(e)), respectively, where currents for probe 1, probe 2, and the sample can be measured simultaneously. I-V curves on these three detectors for 2P-STM with sample open in Fig. S8(b) represent that all current injected by probe 2 is drained into probe 1, thus there is no leak current to the sample detector. On the other hand, the I-V curves for 2P-STM with sample closed show that the current from probe 2 is fractionally drained into probe 1, and that the rest of the current is detected at the sample detector (Fig. S8(d)). In the case of 1P-STM with sample closed, all current from probe 2 flows *via* the surface and is detected at the sample detector, thus there is no current detected at probe 1 (Fig. S8(f)). Considering the roles of each probe and sample on the individual setups, these results are consistent. By comparing the I-V curves measured at probe 2 in Fig. S8(b), (d), and (f), we found that they are almost identical (I-V curves for outside in Fig. S9(b)). We also compared the I-V curves measured with probe 2 inside the U-shaped wire, resulting in that they were almost the same as shown in Fig. S9(b). Thus, this result means that the conductance measured with 1P-STM is equivalent with that with 2P-STM. The conductance measurement with 1P-STM is useful when it is hard or time-consuming to guide the two probes with the separation distance below 1 μm.

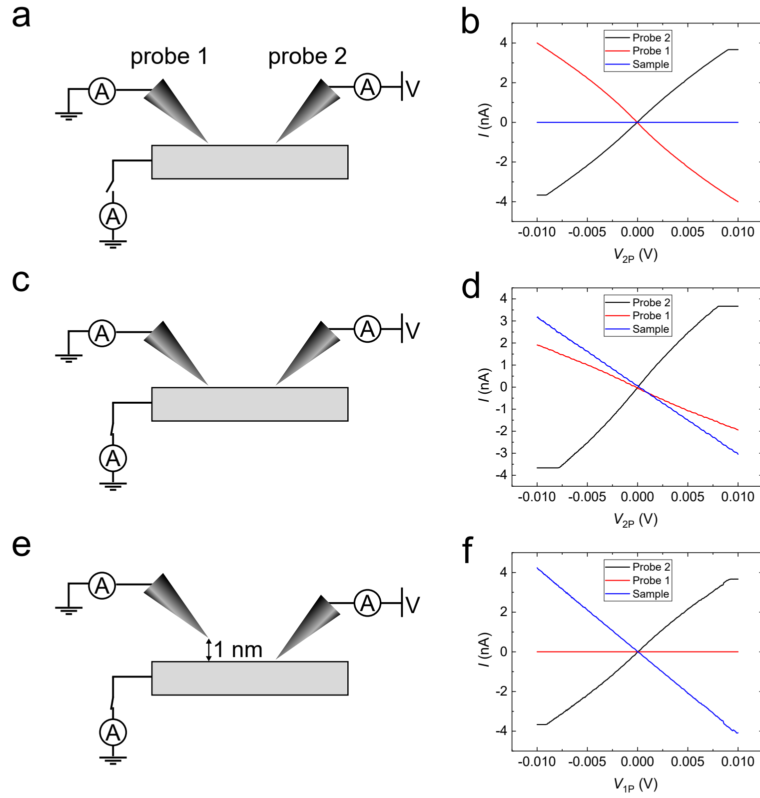

Figure S8: Comparison of I-V curves measured on bare Si surface with 2P- and 1P-STM. Schematics of 2P I-V measurements with sample open (a) and closed (c) and 1P I-V measurement with sample closed (e). (b), (d), and (e) are the sets of I-V curves (simultaneously measured at probe 2, probe1, and sample) for the setups in (a), (c), and (d), respectively.

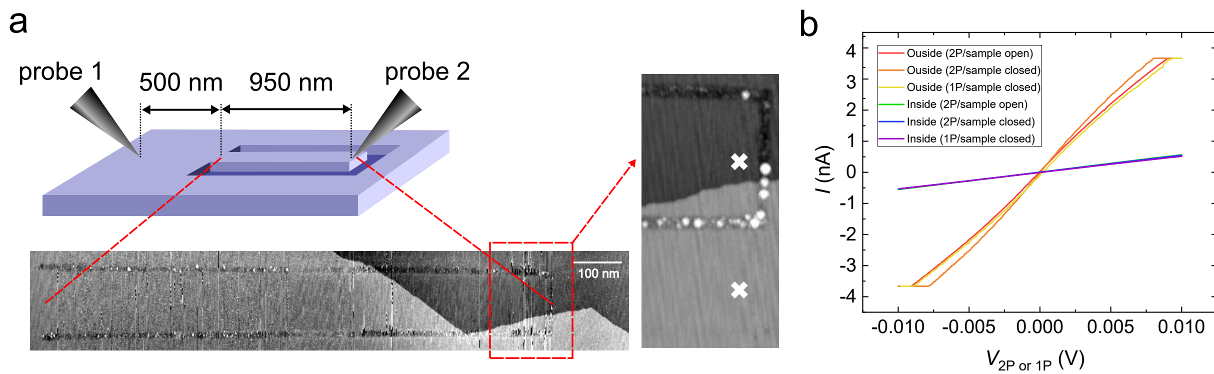

Figure S9: Example of the correspondence between 2P-STM with 1P-STM upon the conductance measurement. (a) Schematics of the 2P- and 1P-STM experiments with the U-shaped wire. STM images show the whole structure of the wire and the measured areas at probe 2. (b) 2P and 1P I-V curves with sample open or closed. The positions of probe 2 for outside and inside of the U-shaped wire are represented in (a) with white crosses.

References

(1) Just, S.; Blab, M.; Korte, S.; Cherepanov, V.; Soltner, H.; Voigtländer, B. Surface and Step Conductivities on Si (111) Surfaces. *Phys. Rev. Lett.* **2015**, *115*, 066801.

(2) Mönch, W. *Electronic Properties of Semiconductor Interfaces*; Springer-Verlag: Berlin, 2004.

(3) Rezeq, M.; Ali, A.; Patole, S. P.; Eledlebi, K.; Dey, R. K.; Cui, B. The Dependence of Schottky Junction (I-V) Characteristics on the Metal Probe Size in Nano Metal-Semiconductor Contacts. *AIP Adv.* **2018**, *8*.

(4) Rezeq, M.; Eledlebi, K.; Ismail, M.; Dey, R. K.; Cui, B. Theoretical and Experimental Investigations of Nano-Schottky Contacts. *J. Appl. Phys.* **2016**, *120*.

(5) Heike, S.; Watanabe, S.; Wada, Y.; Hashizume, T. Electron Conduction through Surface States of the Si(111)-(7×7) Surface. *Phys. Rev. Lett.* **1998**, *81*, 890–893.

(6) Hasegawa, S.; Grey, F. Electronic Transport at Semiconductor Surfaces - From Point-Contact Transistor to Micro-Four-Point Probes. *Surf. Sci.* **2002**, *500*, 84–104.

(7) Hofmann, P.; Wells, J. W. Surface-Sensitive Conductance Measurements. *J. Phys. Condens. Matter* **2009**, *21*.

(8) Nakayama, T.; Kubo, O.; Shingaya, Y.; Higuchi, S.; Hasegawa, T.; Jiang, C.-S.; Okuda, T.; Kuwahara, Y.; Takami, K.; Aono, M. Development and Application of Multiple-Probe Scanning Probe Microscopes. *Adv. Mater.* **2012**, *24*, 1675–1692.

(9) Hasegawa, Y.; Lyo, I. W.; Avouris, P. Measurement of Surface State Conductance Using STM Point Contacts. *Surf. Sci.* **1996**, *357*, 32–37.

(10) Martins, B. V.; Smeu, M.; Livadaru, L.; Guo, H.; Wolkow, R. A. Conductivity of Si (111)-(7× 7): The Role of a Single Atomic Step. *Phys. Rev. Lett.* **2014**, *112*, 246802.

(11) Labidi, H.; Kantorovich, L.; Riedel, D. Atomic-Scale Control of Hydrogen Bonding on a Bare Si (100)-2$\times$ 1 Surface. *Phys. Rev. B* **2012**, *86*, 165441.

(12) Zhang, X.; Wang, K.; Chen, W.; Loy, M.; Wang, J.; Xiao, X. Electrical Transport through a Scanning Tunnelling Microscope Tip and a Heavily Doped Si Contact. *J. Appl. Phys.* **2013**, *114*, 013701.

(13) Onoda, J.; Vick, D.; Salomons, M.; Wolkow, R.; Pitters, J. Consistent Probe Spacing in Multi-Probe STM Experiments. *AIP Adv.* **2020**, *10*, 105213.